Electron tomography based on a Total Generalized Variation minimization reconstruction technique

Ala AlAfeef [*†], Alexander Alekseev[†], Ian MacLaren[†]and Paul Cockshott[*]
* School of Computing Science, University of Glasgow, Glasgow G12 8QQ, United Kingdom.
† School of Physics and Astronomy, Kelvin Nanocharacterisation centre, University of Glasgow, Glasgow G12 8QQ, United Kingdom
E-mail: a.al-afeef.1@research.gla.ac.uk

***Abstract*— Electron tomography (ET) is a key technique for examining the three-dimensional morphologies of nanostructures. ET involves the reconstruction of a set of 2D projection images into a volumetric image by solving an inverse problem. However, due to limitations in the acquisition, reconstruction usually degraded by missing wedge artifacts (e.g., streak, blurring, and elongation artifacts). Assuming piece-wise constant image, total variation minimization has been applied to ET and showed promising results in preserving sharp boundaries. For many samples in Electron microscopy, this assumption is no longer valid causing undesired staircase artifacts. In this work, we describe the application of Total Generalized Variation (TGV) to ET reconstruction under CS theorem and demonstrate the effectiveness of CS-TGV to produce results with higher fidelity using simulation and experimental study.**

I. INTRODUCTION

In materials science, Electron tomography (ET) is considered an effective technique that provides indispensable information for the study of particles and structures in the Nanoworld. The 3D morphology of nanostructures can be provided by reconstructing an aligned set of 2D TEM images acquired around a single or double tilting axis. The reconstruction step in ET is performed using image reconstruction algorithm such as weighted back projection (WBP) or simultaneous iterative reconstruction technique (SIRT). SIRT algorithm provides reconstruction of a relatively higher Signal-to-noise ratio than those obtained using WBP. However, the reconstruction still suffers from elongation, blurring and artifacts due to the missing wedge limitation in ET. The number of projections that can be recorded is limited by the maximum tilt angle (typically ±72 degrees) above which projections cannot be acquired. A segmentation step is usually needed to overcome such artifacts and to distinguish between artifacts and main components in the reconstruction. This segmentation process is often performed manually leading to a potentially subjective and time-consuming interpretation of the data.

The reconstruction process of ET can be explained by considering a 3D object as a set of 2D sections. The reconstruction of that object can then be created by reconstructing each 2D section from the corresponding 1D projection. An object may be reconstructed from its projections by inverting the projection process which, in the presence of noise, can be modelled as:

$$b = Au + \eta \qquad (1)$$

Where A is the discrete Radon transform that projects the real object u (2D imaged object) into measurements b (1D-projections) and η is an error term modeling noise in the measurements. To conduct a reconstruction (tomogram), the unknown vector u needs to be recovered from measurements b. However, due to limitations in the acquisition process, this inverse problem is ill-posed (i.e. unique solution may not exist). Also, the reconstruction will be further degraded with the presence of noise and alignment errors.

A technique has recently been developed, named compressive sensing (CS) [11-12] which created a complete paradigm shift to the area of sampling. CS provides a theoretical justification for the possibility recovering an under-sampled signal at lower sampling rate than that required by the Nyquist sampling theorem. With the assumption, that the signal is sparse in a selected domain (i.e. DCT, Wavelet, etc.), it is possible to reconstruct a signal at high quality. CS has been applied with great success in Magnetic Resonance Imaging (MRI) [5] and more recently been applied to ET [13-18]. It has been demonstrated that, even with reduced datasets, it is possible to reconstruct tomograms with high fidelity and a reduced missing wedge artifacts [14]. Such promising advantages make CS an effective method for reducing beam damage, obtaining reliable, high-resolution morphology, and enabling quantitative measurements from 3D tomograms. The quality of a tomographic reconstruction can be enhanced by including additional prior knowledge about the specimen throughout the reconstruction process.

The key prior knowledge employed in CS is that the signal likely to be sparse in a transform domain. One common sparsifying transform in CS image processing is spatial finite-differences. Sparsity in finite differences is evaluated as the $\ell 1$-norm of the Discrete Gradient Transform (DGT) coefficients of an image, which is often referred to as the Total Variation (TV) [24]. TV is well-known in image restoration problems like denoising [1], CS [2], [3] and has been suggested for tomographic reconstruction in ET problem [5, 9, 10]. Saghi et al. in [14, 15] were able to recover iron oxide nanoparticles (i.e., object with concave surfaces morphology) with only 9 projections.

In spite of the success of TV, it performs best with piece-wise constant images, which can damage fine details, and cause staircase artifacts in reconstructions [4,19]. As a solution, Total Generalized Variation (TGV) [4,6,23] was proposed and become more popular in image restoration as a means to overcome staircase artifacts. In this paper, we validate the efficiency of TGV for the ET reconstruction problem through experimental results and test both noisy and noiseless cases in comparison with other established ET techniques.

The paper is organized as following. Section II gives a brief introduction to Total Variation and its associated staircase artifacts. In order to overcome this drawback, the generalized version of TV, TGV, is delivered in Section III. In section IV and V, reconstructions using TGV is compared to TV and other established recovery methods in the ET problem using noisy/noisy-free experiments as well as with real data. Finally, conclusions in given in Section VI.

II. TOTAL VARIATION MINIMIZATION (TVM) BASED RECONSTRUCTION TECHNIQUE

Among many sparsifying techniques, the well-known total variation minimization (TV) has been adopted to solve many problems in image processing such as denoising and tomography [14,19] with a promising capability to preserve sharp edges. Theoretical proof for TV is given in [8]. Due to the nature of ET images which are approximately sparse in the gradient domain; CS can be applied by minimising the gradient norm in the ET image reconstruction problem similar to [5]. In ET, tomogram can reconstruct by using following optimization:

$$\hat{u} = \text{argmin}_u \ \|Au - b\|_2^2 + \lambda_{TV} TV(u) \qquad (2)$$

where $\lambda_{TV} > 0$ denotes regularization parameter and anisotropic version formulated as $TV(u) = \int_{\Omega} \|\nabla u\|_p dx$. The notation Ω denotes an open, convex, connected and non-empty set in $\mathbb{R}^d$, ∇ represents gradient operator and L_p norm is defined as $\|v\|_p = (\sum_{i=1}^{N}(v_i)^p)^{1/p}$. Norm p equals 1 or 2 for anisotropic and isotropic TV, respectively.

To improve reconstruction performance, TV was further combined with an L_1 cost function in [5] as following:

$$\hat{u} = \text{argmin}_u \ \|Au - b\|_2^2 + \lambda_{L1}\|\Psi u\|_1 + \lambda_{TV} TV(u) \qquad (3)$$

λ_{L1} is another regularization parameter to provides a balance between the loss of fine details and the elimination of ghosting artifacts. This landmark paper in [5], produced the current state of the art reconstruction method for MRI, and was further applied to ET as in [9,10].

III. TOTAL GENERALIZED VARIATION MINIMIZATION (TGVM) BASED RECONSTRUCTION TECHNIQUE

Although using TV is successful in preserving sharp edges and outperform established ET reconstruction methods (such as, WBP and SIRT), it causes an undesirable artifact namely, staircase artifact as can be seen in Fig. 1. Many efforts have been made to overcome this limitation such as: nonlocal TV [1], nonlocal regularization [2], higher order TV [3].

More recently, the TGV [4,6,7] as a generalized version of TV has been proposed. Instead of considering only first order

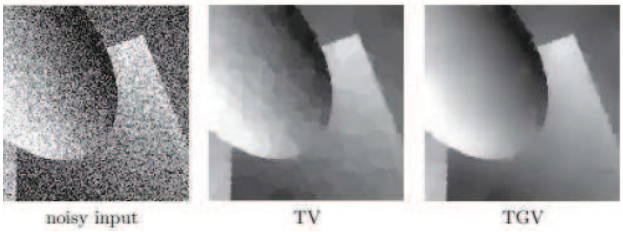

Figure. 1. Image denoising results Comparison of TV and TGV, extracted from [4]

derivatives as in TV, TGV involves orders >= 2 . Compared to TV, TGV preserves edges better due to the minimization of errors in higher derivatives. Therefore, with TGV regularization, image detail is well preserved as shown in Fig. 1. In the context of ET, the reconstruction of TGV can be accomplished by the following optimization problem:

$$\hat{u} = \text{argmin}_u \ \|Au - b\|_2^2 + \frac{\mu}{2} TGV_\alpha^k(u) \qquad (4)$$

Where TGV_α^k of order k and positive weights $\alpha = (\alpha_0, \dots, \alpha_{k-1})$ incorporates multiple order derivative as

$$TGV_\alpha^k(u) = sup\left\{ \int_\Omega u \, \text{div}^k \omega \ dx \mid \omega \in C_c^k\left(\Omega, \text{Sym}^k(\mathbb{R}^d)\right), \ \|\text{div}^l \omega\|_\infty \le \alpha_l, l = 1,2, \dots k-1 \right\}$$

Notation $C_c^k\left(\Omega, Sym^k(\mathbb{R}^d)\right)$ is the space of compactly supported symmetric tensor field and $\text{Sym}^k(\mathbb{R}^d)$ denotes the space of symmetric tensor of order k on $\mathbb{R}^d$. By setting $k = 1, \alpha = 1$, TGV_1^1 is nothing but exactly TV. In case of $k = 2$, the second order of TGV_α^2 is given as

$$TGV_\alpha^{k=2}(u) = sup\left\{ \int_\Omega u \, \text{div}^2 \omega \ dx \mid \omega \in C_c^2(\Omega, S^{d\times d}), \ \|\omega\|_\infty \le \alpha_0, \|\text{div}\, \omega\|_\infty \le \alpha_1 \right\}$$

where the divergences and infinity norms are defined as

$$(\text{div}\, \omega)_i = \sum_{j=1}^{d} \frac{\partial \omega_{ij}}{\partial x_j};$$

$$\text{div}^2 \omega = \sum_{i=1}^{d} \frac{\partial^2 \omega_{ii}}{\partial x_i^2} + \sum_{i<j} 2 \frac{\partial^2 \omega_{ij}}{\partial x_i \partial x_j}$$

$$\|\omega\|_\infty = \sup_{l\in\Omega} \left(\sum_{i,j=1}^{d} \left|\omega_{ij}(l)\right|^2 \right)^{1/2}$$

$$\|\text{div}\, \omega\|_\infty = \sup_{l\in\Omega} \left(\sum_{i,j=1}^{d} \left|(\text{div}\, \omega)_j(l)\right|^2 \right)^{1/2}$$

We can further refine the formula of TGV_α^2 as minimum of all complex vector field ω

$$TGV_\alpha^2(u) = \text{argmin}_v \ \alpha_1 \|\nabla u - \omega\|_1 + \alpha_0 \|\mathcal{E}(\omega)\|_1 \qquad (5)$$

where $\mathcal{E}(\omega) = \frac{1}{2}(\nabla\omega + \nabla\omega^T)$ represent the symmetrized gradient of a complex-valued vector field . An example of TGV_α^2 minimizing higher orders of variation, and reducing staircase artifact is shown in Fig. 1. We found parameter settings $\alpha_1 = 1$ and $\alpha_0 = 2$ provided the optimal performance in practice as suggested in [4, 6]. In this paper, we adopt the solver [6] for TGV_α^2 which use primal-dual methods and its C++ and CUDA implementation in the AGILE package [7].

IV. Simulation Results

To evaluate performance, simulation was performed using a phantom image (Fig. 2, first row) and (Fig. 3a). The first phantom includes a large "hole" with intensity varying inversely with square of radius in the background, while the second contains sixteen low-contrast disks of varying radii. Both phantoms are not sparse under a gradient transformation. Such phantoms with a gradual intensity variation can simulate realistic materials in a normal TEM experiment such as solar cells [20] as in experimental TEM images in Fig. 4. To provide completed comparison, simulations were performed at different under-sampling factors, and noise setting. Moreover, the experimental test in real ET data was performed on tilt series similar to Fig. 4(A).

For comparisons, we compared the proposed algorithm with established techniques in ET namely, WBP, SIRT[21] and state of the art CS-based Total variation (CS-TV)[5,14]. The output is assessed in terms of two commonly used metrics: Peak Signal-to-Noise Ratio (PSNR) and Structural SIMilarity (SSIM) index. All implementations were executed on Matlab v7.12 (R2011a) installed on a 64-bit Windows 7 operating system with an Intel Core i5 processor running at 3.10 GHz with 24 GB memory and NVIDIA GeForce GTX 460 with Cuda compiler V4.1.

A. Experiment Setting

In order to avoid committing 'inverse crimes', which happens when the data is inappropriately simulated [22], the tilt series were generated using the parallel projection discrete Radon transform, while reconstruction was coded using Fourier-based methods so that a different system matrix is used for creating projections than in the reconstruction methods. Furthermore, the tilt series was misaligned by randomly shifting each projection by a maximum of $\pm 0.5^{\circ}$ to account for the alignment imperfection of experimental ET data. This gives a more realistic simulation of the problems present in real ET data. The input data in each case was then prepared by taking the 1D Fourier transform of each projection in a tilt series and sampling it to the corresponding radial line in the 2D Fourier domain followed by an inverse transform.

The WBP reconstruction was performed with a Ramp filter, and used to initialize other algorithms. SIRT was performed using 32 iterations. CSTV reconstruction was performed using the method provided by Lustig et al [5] seeking sparsity in the gradient and image domains with default regularization weighting of λ_{TV} = 6 and λ_{L1} = 1, respectively. In case of CS-TV, 150 conjugate gradient iterations were performed with a re-initialization every 50 iterations to decreasing the likelihood of falling into local minima.

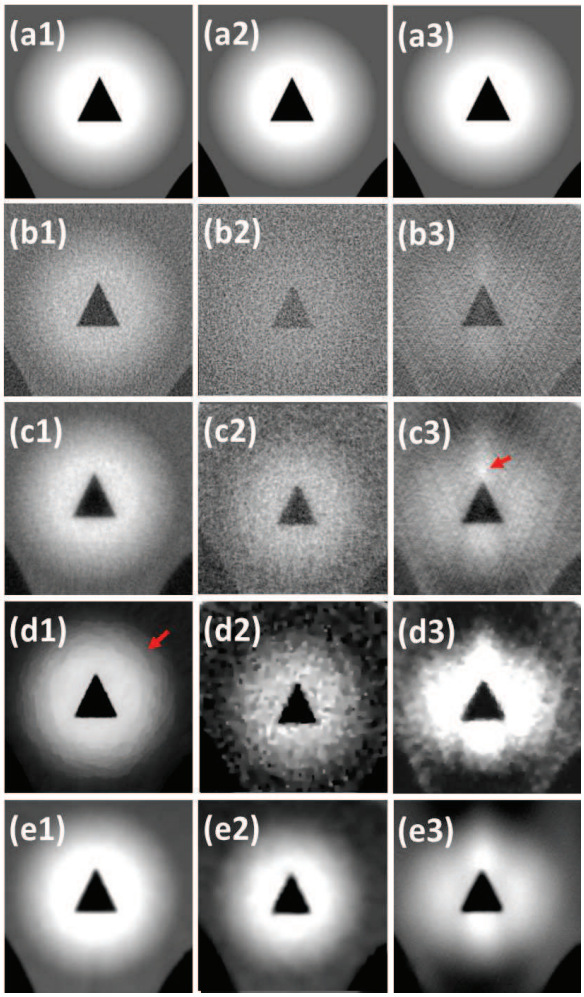

Figure. 2. Comparison between results of ET recovery methods - first and second columns is a reconstruction from denoising case (Setup 1 and 2 respectively), last column, shows reconstruction from under-sampling case (setup 3) (row images: a-ground truth with 256^2 pixels, reconstructed using b-WBP, c-SIRT, d-CSTV, e-TGV). a1-a3 are identical images viewed for convenience.

B. Denoising Case

As denoising is the natural application of both TV and TGV, in this section, the performance of CS-TGV is evaluated for noisy cases. Three simulation setups were generated. Setups 1 and 2: high angular sampled projections with low level of noise. Phantom in Fig. 2a was projected into the sinogram domain between $\pm 90^{o}$ with 1^{o} tilt increment. This was then corrupted by applying 1) Poisson noise to simulate the shot noise and 2) Gaussian noise with low (left column in Fig. 2) and high (middle column in Fig. 2) standard deviations σ, to reach a SNR of 52dB and 15dB, respectively. In Setup 3: low angular sampled projections were simulated between $\pm 70^{o}$ with 5^{o} tilt increment and corrupted by shot noise (right column in Fig. 2).

TABLE I. PSNR AND SSIM QUALITY VALUSES OF RECONSTRUCTION USING VARIOUS METHODS GIVEN IN FIG.2.

Fig. 2	Left Column		Middle Column		Right Column		Run time
Method	**PSNR**	**SSIM**	**PSNR**	**SSIM**	**PSNR**	**SSIM**	***Secs***
WBP	14.4	0.17	8.2	0.08	10.6	0.09	7
SIRT	20.8	0.34	12.7	0.15	15.7	0.23	54
CS-TV	21.3	0.85	14.4	0.31	17.3	0.36	96
CS-TGV	**21.9**	**0.90**	**19.2**	**0.81**	**18.4**	**0.61**	**102**

As can be seen in Fig. 2, the WBP result is heavily contaminated with noise, SIRT produces slightly better performance with less noise but also blurs the sharp edges. CS-TV instead produces much higher performance especially in preserving sharp edges and removes noise (to a certain degree). However, staircase artifacts are apparent (arrow in Fig.2-d1) in the smooth region. The results produced by CS-TGV show a higher visual similarity to the test phantom with reduced staircase artifacts. The edges are preserved and noise is removed while staircase artifacts are hardly visible. Also, the missing wedge artifact was further suppressed in both CS-TV and CS-TGV based methods. However, limited blurring can be still observed in CS-TGV results at the edges region in comparison with CS-TV(see Fig. 2-d2 and e2). It is because CS-TV uses more prior information about sparsity in transform and gradient domains as combination of TV and L1 minimization. Therefore, there still is a room for further improved CS-TGV performance. Table. I shows the quality index results for various reconstruction method given in Fig. 2.

C. Undersampled case

In addition to Fig.2(a3-e3), in this section, we evaluate the performance of various algorithms in the presence of missing projections. This is also considered as under-sampling problem or generally a compressive sensing problem. In this experiment, the CS-phantom proposed in [22] was projected into the sinogram domain between ±70° with 5° tilt increment and then reconstructed using WBP, SIRT and CS-TGV. Fig. 3a shows the top left part of the reconstruction. CS-phantom is designed for testing the accuracy of CS solvers and the properties of CS reconstruction artifacts. As a consequence of the reduced number of projections, lower recovery performance is obtained. From this data, CS-TGV still provides the best recovery performance as we expected. Furthermore, streak artifact was reduced for these low-contrast features.

V. MORPHOLOGY STUDY OF POLYMER BLEND SAMPLE

In this section, the CS-TGV is used to study the morphology of solar cell (particularly the PTB7:PC71BM blends). The performance of such blends critically depends on the nanoscale organization and morphology of its particles. This is why ET is an important tool to identify the local volume morphology with a nanometer resolution in order to improve its efficiency. For this purpose, a tilt series was acquired for a thin section of the polymer blend with thickness range between (120 to 150nm) making it electron transparent which is important to avoid shadowing at higher tilts. Electron microscopy was performed on FEI Tecnai T20 TEM. The Energy-filtered transmission electron microscopy (EFTEM) imaging mode was chosen. A tilt series was acquired over a tilt range of 62°, with an increment of 2° between consecutive projections. More details about imaging condition can be found in [20]. Fig. 4 (b-e), shows XY-orthogonal slice taken at the middle of reconstructed volume using different methods. The CS-TGV slice shows a reconstruction with higher fidelity for this noisy and reduced dataset. CS-TV results can be improved to reduce noise, by increasing the λ_{TV} term in (3), however, this will be at the cost of losing fine details. Such limitation can be avoided by using CS-TGV method.

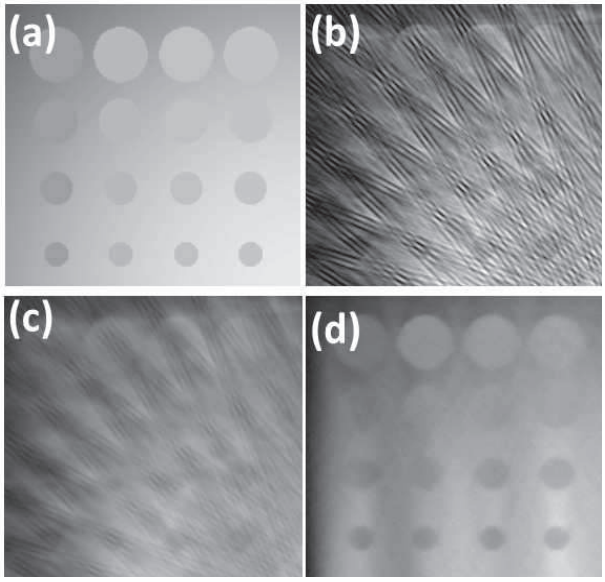

Figure. 3. Reconstruction results of Under-sampling case - a) Ground truth with 256^2 pixels, compared to results using b)WBP, c)SIRT and d) TGV.

VI. CONCLUSION

In this paper, the efficiency of TGV minimization for ET reconstruction problem is validated for noisy and under-sampled dataset. In both cases, TGV outperforms TV and traditional methods in term of objective and subjective quality. Staircase artifact and noise is significant reduced in CS-TGV. This will allow for a reconstruction with higher fidelity which is important for to determine the organization and morphology of nanoscale particles.

ACKNOWLEDGEMENT

This research was supported by a Lord Kelvin Adam Smith Scholarship of the University of Glasgow. We would like to thank Thuong Nguyen for the fruitful discussion.

References

[1] X. Zhang, M. Burger, X. Bresson, and S. Osher, "Bregmanized Nonlocal Regularization for Deconvolution and Sparse Reconstructions," *SIAM J. Imag. Sci.*, vol. 3, no. 3, pp. 253-276, 2010.

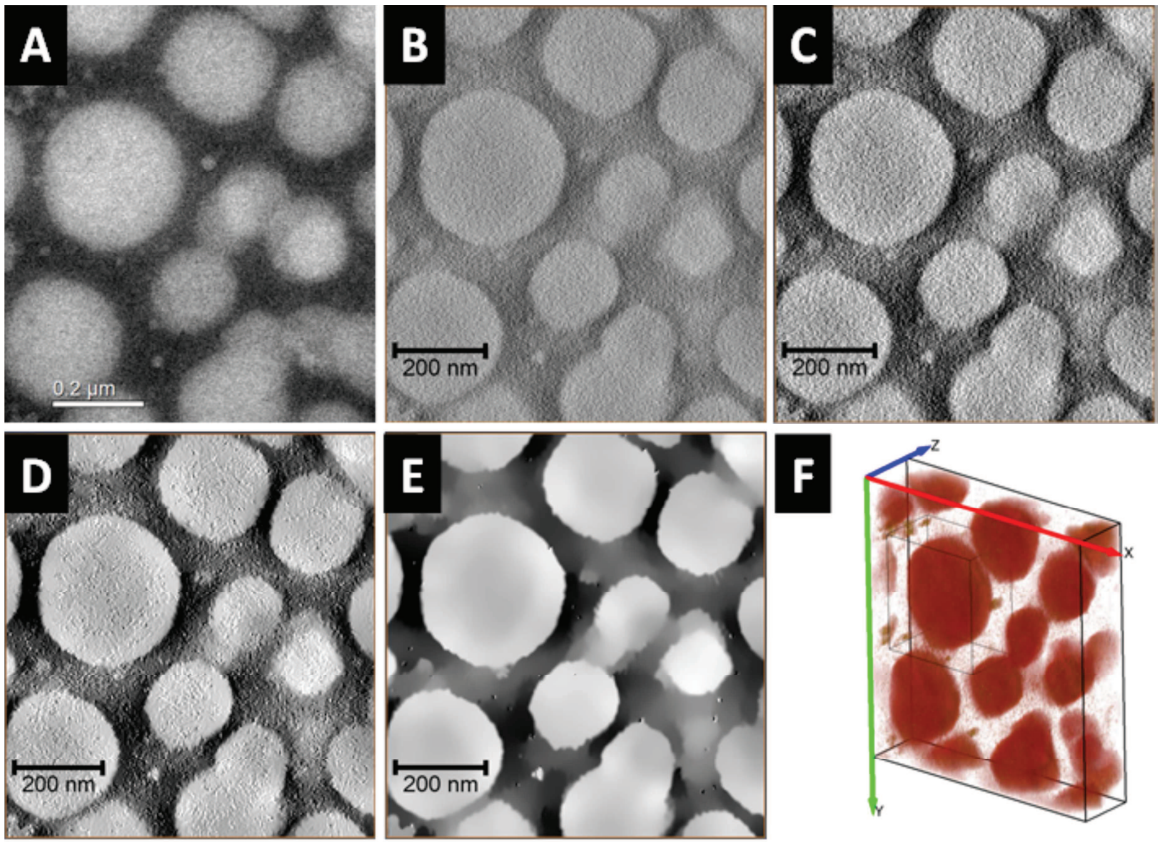

Figure. 4. Solar cell Electron Tomography - A) TEM tilted image acquired at 0 tilt angle acquired using EFTEM imaging. The tilt series is reconstructed using) WBP, C) SIRT, D)CS-TV and E) CS-TGV. F) Volume rendering of CS_TGV result.

[2] Y. Hu and M. Jacob, "Higher Degree Total Variation (HDTV) Regularizaiton for Image Recovery," *IEEE Trans. Image Process.*, vol. 21, no. 5, pp. 2559-2571, 2012.

[3] T. N. Canh, K. Q. Dinh, and B. Jeon, "Total variation reconstruction for Kronecker compressive sensign with a new regularization," *IEEE Pic. Coding Symp.*, pp. 261-264, 2013.

[4] K. Bredies, K. Kunisch, and T. Pock, "Total generalized variation", *SIAM J. Imaging Sci.*, vol. 3, pp. 492-526, 2010.

[5] M. Lustig, D. Donoho, and J. M. Pauly, "SparseMRI: The application of Compressed sensign for MR Imaging," *J. Mag. Reson. Med.*, pp.1522-2594, vol. 58, no. 6, 2007.

[6] F. Knoll, K. Bredies, T. Pock, and R. Stollberger, "Second Order Total Generalized Variation (TGV) for MRI," *J. Mag. Reson. Med.*, vol. 65, no. 2, pp. 480-491, 2011.

[7] M. Freiberger, F. Knol et.al., "The Agile Library for Biomedial Image Reconstruction using GPU," *IEEE J. Comp. Sci. Engin.*, vol. 15, no. 1, p. 34-44, 2013.

[8] D. Needell,R. Ward,"Stable Image Reconstruction Using Total Variation Minimization," *SIAM J. Imag. Sci.*,vol 6, no. 2, pp.1035-1058, 2013.

[9] B. Goris, W. V. Broek, K.J. Batenburg, H. H. Mezerji, and S. Bals, "Electron tomography based on a total variation minimization techniques," *Ultramicroscopy*, vol. 113, pp. 120-130, 2012.

[10] R. Leary, Z. Saghi, P. Midgley, and D. J. Holland, "Compressed senisng electron tomography,"*Ultramicroscopy*, vol.131, pp.70-91, 2013.

[11] D. L. Donoho, "Compressed sensing," IEEE Trans. Info. Theory, vol. 52, no. 4, pp. 1289–1306, 2006.

[12] E. J. Candes and M. B. Wakin, "An introduction to compressive sampling," *IEEE Signal Process. Mag.,* vol. 25, no. 2, pp. 21–30, 2008.

[13] P. Binev, W. Dahmen, R. DeVore, P. Lamby, D. Savu, and R. Sharpley, "Compressed sensing and electron microscopy," *Nonostructure Sci. Tech.*, 2012.

[14] Z. Saghi, D. J. Holland, R. Leary, A. Falqui, G. Bertoni, A. J. Sederman, L. F. Gladden, and P. A. Midgley, "Three-dimensional morphology of iron oxide nanoparticles with reactive concave surfaces" *Nano Letters*, vol. 1, no. 11, pp. 4666–4673, 2011.

[15] R. Leary, Z. Saghi, P. A. Midgley, and D. J. Holland, "Compressed sensing electron tomography,"*Ultramicroscopy*,vol.131,pp.70–91, 2013.

[16] N. Monsegue, X. Jin, T. Echigo, G. Wang, and M. Murayama, "Threedimensional characterization of iron oxide nanoparticles" *Microscopy and Microanalysis*, vol. 18, pp 1362–1367, 2012.

[17] A.Stevens, H.Yang, L. Carin, I. Arslan, and N. Browning, "The potential for bayesian compressive sensing to significantly reduce electron dose in high-resolution stem images," *Microscopy*,, 2013.

[18] A. AlAfeef, P. Cockshott, I. MacLaren, and S. McVitie, "Compressed sensing electron tomography using adaptive dictionaries: a simulation study," *IOP Publishing J. of Physics: Conf. Series*, vol. 522, no. 1, 2014.

[19] V. Caselles, A. Chambolle, and M. Novaga, "The discontinuity set of solutions of the tv denoising problem and some extensions," *Mul. Model. & simul.*, vol. 6, no. 3, pp. 879–894, 2007.

[20] Alekseev, A., Hedley, G. J., Al-Afeef, A., Ageev, O. A., & Samuel, I., "Morphology and local electrical properties of PTB7: PC71BM blends." J. Mater. Chem. A (in press), 2015.

[21] P. F. C. Gilbert, "The reconstruction of a three-dimensional structure from projections and its application to electron microscopy" *Proc. of the Royal Society of London. Series B. Biological Sciences*, vol. 182, no. 1066, pp. 89–102, 1972.

[22] Leiserson, Charles E., Ronald L. Rivest, and Clifford Stein. Introduction to algorithms. *Ed. Thomas H. Cormen. MIT press*, 2001.

[23] Ono, S., Yamada I., "Second-order total generalized variation constraint" Proc. Int. Conf. Acoust., Speech Signal Process., pp. 4938-4942, May 2014, Florence, Italy.

[24] L. Rudin, S. Osher, E. Fatemi, "Non-linear total variation noise removal algorithm", Physica D: Nonlinear Phenomena 60 (1992) 259–268.